The carbon dioxide evasion cycle of an intermittent first-order stream: Contrasting water-air and soil-air exchange

Arún Looman [a,b]*, Damien T. Maher [a,b], Elise Pendall [c], Adrian Bass [c,d], Isaac R. Santos [a,b]

[a]*National Marine Science Centre, Southern Cross University, Coffs Harbour, New South Wales, Australia.*

[b]*School of Environment, Science, and Engineering, Southern Cross University, Lismore, New South Wales, Australia.*

[c]*Hawkesbury Institute for the Environment, Western Sydney University, Richmond, New South Wales, Australia.*

[d]*Department of Geographical and Earth Sciences, University of Glasgow, Glasgow, United Kingdom.*

Corresponding author E-mail address: arun.looman@hotmail.com

Keywords: Ephemeral, Greenhouse gas, Methane, Headwater stream, Air-water flux

Journal name: Biogeochemistry.

Acknowledgements: Special thanks are given to V. Kumar and C. Barton of Western Sydney University (UWS), the Blue Mountains City Council (BMCC), C. Holloway (SCU), and W. Davis for their assistance with logistics. We acknowledge funding from the Australian Research Council (LE120100156, DE140101733 and DE150100581).

Abstract

Ephemeral streams and wetlands are characterized by complex cycles of submersion and emersion, which influence the greenhouse gas flux rates. In this study we quantify the spatiotemporal variability in CO_2 and CH_4 concentrations and fluxes of an intermittent first-order stream over three consecutive wet and dry cycles spanning 56 days, to assess how hydrologic phase transitions influence greenhouse gas evasion. Water column excess CO_2 ranged from -11 to 1600 μM, and excess CH_4 from 1 to 15 μM. After accounting for temporal changes in the ratio of wet versus dry streambed hydraulic radius, total CO_2-C fluxes ranged from 12 to 156 mmol m^{-2} d^{-1}, with an integrated daily mean of 61 ± 25 mmol m^{-2} d^{-1}. Soil-air evasion rates were approximately equal to those of water-air evasion. Rainfall increased background water-air CO_2-C fluxes by up to 780% due to an increase in gas transfer velocity in the otherwise still waters. CH_4-C fluxes increased 19-fold over the duration of the initial, longer wet-cycle from 0.1 to 1.9 mmol m^{-2} d^{-1}. Temporal shifts in water depth and site-specific ephemerality were key drivers of carbon dynamics in the upper Jamison Creek watercourse. Based on these findings, we hypothesize that the cyclic periodicity of fluxes of biogenic gases from frequently intermittent streams (wet and dry cycles ranging from days to weeks) and seasonally ephemeral watercourses (dry for months at a time) are likely to differ, and therefore these differences should be considered when integrating transient systems into regional carbon budgets and models of global change.

Introduction

The exchange of carbon dioxide (CO_2) and methane (CH_4) between inland waters and the atmosphere is a dynamic process. Variability in the fluxes of CO_2 and CH_4 at the water- and soil-to-air interfaces is influenced by multiple factors including seasonality (Rudorff et al. 2011; Peter et al. 2014), atmospheric forcing (e.g. rainfall, wind velocity; Frew et al. 2004; Ho et al. 2007; Dinsmore and Billett 2008), stream hydraulics (Alin et al. 2011; Raymond et al. 2012), groundwater discharge (Jones and Mulholland 1998; Sadat-Noori et al. 2015), and metabolism (Tamooh et al. 2013). In flowing waters, the partial pressure of CO_2 (pCO_2) can vary over orders of magnitude both spatially (Koprivnjak, et al. 2010; Weyhenmeyer et al. 2012; Teodoru et al. 2015), and temporally (Johnson et al. 2007; Bass et al. 2014; Ruiz-Halpern et al. 2015; Looman et al. 2016; Tweed et al. 2016). This variability, along with a limited extent of available data and the lack of a modelling framework for many aquatic systems (Raymond et al. 2013; Regnier et al. 2013), complicates the quantification of greenhouse gas (GHG) emissions from inland waters as well as our understanding of their role in the global carbon (C) cycle (Battin et al. 2009). Seasonally ephemeral and frequently intermittent low order streams are components of the fluvial network, and to date there is limited understanding on the spatial and temporal variability of water- and soil-to-air GHG exchange rates in these systems (von Schiller 2014).

Temporary watercourses can comprise more than 50% of the total drainage network length within water catchments (Hansen et al. 2001; Nadeau and Rains 2007), and are particularly common to headwaters (Costigan et al. 2015). The extent of

perennial vs. non-perennial segment length in these systems is, however, not constant, due to a cyclic continuum of network extension, contraction and fragmentation (von Schiller et al. 2015). In landscapes where discontinuity of flow is particularly pronounced even Strahler order delineations (Strahler 1957) can be dynamic, shifting by up to two orders between seasonal extremes (Datry et al. 2014; Godsey and Kirchner 2014). For unregulated rivers, Haines et al. (1988) described 15 seasonally-based flow regime classes, of which three describe the natural zero-flow sequences commonly found in Australia (McMahon and Finlayson 2003): (i) perennial streams with high annual variability that cease to flow in extreme years; (ii) ephemeral streams that regularly cease to flow in the dry season; and (iii) arid zone streams with long and erratic periods of no flow.

In non-perennial watercourses the frequency and duration of natural hydrologic fragmentation relates to site-specific attributes such as annual precipitation, ambient temperature, riparian vegetation-streamflow interactions, watercourse shade dynamics, topography, slope, geomorphology, groundwater levels and sedimentology (Leopold and Maddock, 1953; Shaw and Cooper 2008; Salemi et al. 2012; Snelder et al. 2013). In anthropogenically-modified environments, the wet and dry cycle recurrence interval can be further influenced by factors such as urbanization (impermeable surfaces), the presence/absence of serial discontinuities (e.g. weirs, impoundments), and groundwater or surface water abstraction (Holmes 1999; Stanford and Ward, 2001; Steward et al. 2012). McMahon and Finlayson (2003) use the term “anti-drought” to describe the regulated addition of larger or more persistent flows to the natural hydrologic regime during dry or low-flow intervals, resulting in artificial wet and dry cycle intermittence.

Hydrologic phase transitions such as that from baseflow to stormflow can give rise to hot spot and hot moment phenomena of accelerated rates in the spiralling of dissolved carbon and nutrients in perennial inland waters (McClain et al. 2003; Hook and Yeakley 2005; Raymond and Saiers 2010; Janke et al. 2014; Raymond et al. 2016). In ephemeral watercourses, other transitions such as streambed drying and rewetting can alter the rates of macromolecular decomposition (Dieter et al. 2011), biofilm metabolism and community structure (Timonser et al. 2012; Fazi et al. 2013; Sabater et al. 2016), as well as connectivity between adjacent pools (Larned et al. 2010; Bernal et al. 2012; Casas-Ruiz et al. 2016). The coupled influence of such transition processes on the rate of GHG fluxes from ephemeral waters, however, remains largely unknown. In the present study, we quantify the spatial flux as well as temporal changes to the CO_2 and CH_4 dynamics of an intermittent first-order stream (Jamison Creek, Blue Mountains, Australia) over three consecutive wet and dry cycles occurring over a 56-day period. Our primary objectives were: (i) to quantify variability in CO_2 emissions from wet versus dry portions of the stream reach during episodes of expansion and contraction; (ii) to assess changes in CO_2 and CH_4 fluxes within the study segment over time; and, (iii) to evaluate the significance of rain events on GHG emissions.

Methods

Study site

Field investigations were performed in the headwaters of the upper Jamison Creek water

116 catchment in the Greater Blue Mountains World Heritage Area of New South Wales,
117 Australia (33°42'S, 150°22'E; 867 mASL; Fig. 1), west of the Sydney Basin. The mean
118 annual ambient temperature at the nearest meteorological station in Katoomba is 12.4 ±
119 4.4 °C and mean annual precipitation 1405 ± 35 mm (1885–2016 period; Station
120 #063039; BoM 2015a). There are on average 162 days influenced by rainfall annually,
121 with mean rainfall rates of ≥1, ≥10 and ≥25 mm d^{-1} for 108, 39 and 15 days, respectively.
122 The catchment sediments are derived from Hawkesbury and Narrabeen Group
123 sandstones and are predominantly siliceous, with localised peat deposits and claystone
124 interbeds (Fryirs et al. 2016). Streambed sediments are of sandy-loam textural class, with
125 occasional Fe mottles indicative of changeable hyporheic zone redox chemistry. In-
126 stream flora was dominated by *Cyperus eragrostis* and *Rumex obtusifolius*. Vegetative
127 coverage of the less-frequently inundated upstream study segments (sites S1 and S2, see
128 below for details) varied from ~20% in winter to ~50% by the end of the sampling period
129 in mid-spring. The more-frequently inundated downstream study segments were, in
130 contrast, void of in-stream vegetation. During the wet cycles, biofilms and filamentous
131 chlorophytes were also present.
132
133 Experimental approach
134
135 Measurements were taken from the uppermost 100 m of the watercourse, which has been
136 modified (e.g. straightened) to connect a 36 ha golf course to Lake Wentworth, a flooded
137 Temperate Highland Peat Swamp on Sandstone (an endangered ecological community;
138 TSSC 2005). The study segment was further reduced to five shorter sub-reaches spanning

139 5.7 to 20.1 m in length (sites S1-S5; Fig. 1) according to conditions of observed
140 disconnection during periods of low stage height. For time series observations, all data
141 were collected at the upstream S1 site over a 56-day time period during the winter-spring
142 transition (23 August – 17 October, 2015; modified channel), and, for spatial
143 observations, all sites were surveyed during two separate wet-cycles when the stream was
144 disconnected (11/9 and 21/09; Table 1). Study segment S2 was located inside a roadway
145 culvert and sites S3-S5 represented a channelised, non-flooded section of the peat swamp.
146 We sampled pH, conductivity, temperature, and dissolved oxygen (DO)
147 concentrations *in-situ* with a Hydrolab DS5X multiparameter sonde. pH and conductivity
148 were calibrated against pH_{NBS} buffers 4.00 and 7.00 and conductivity against a 1410 μS
149 cm^{-1} solution. The sonde was recalibrated at the start and end of each rewetting cycle.
150 Ambient temperature, wind speed, rainfall rate and barometric pressure were measured
151 with a portable weather station fitted with a cup anemometer (Davis Instruments, USA),
152 located central to the Jamison Creek catchment 1.2 km from the study site.
153 Evapotranspiration data was obtained from the Mount Boyce meteorological station
154 (33°36'S, 150°16'E; Station #063292; BoM, 2015b), 14.5 km away.
155 To account for temporal changes in the ratio of wet versus dry surface area, we
156 measured stream depth and width at 30 x 30 cm intervals under conditions of high stage
157 (i.e. using the water level as a reference datum) to create a detailed bathymetric digital
158 elevation model (DEM) of the study segment. Relative change in stage height (positive or
159 negative) was recorded at a fixed datum in sub-reach S1, and, using this datum, we then
160 determined the subsequent mean wetted channel width (w, m), mean water depth (d, m),
161 water volume (V, m^3), and water-to-soil ratios for each sampling interval. To estimate

streamwater velocity, we formulated a discharge-rating curve from the continuity relationship $Q = dwv$ and interpolated v from gauge heights above $Q = 0$ via cubic polynomial function (Xia et al. 2010), where Q is the discharge in $m^3\ s^{-1}$ and v is velocity in $m\ s^{-1}$.

Dissolved gas analyses

Streamwater pCO_2 and pCH_4 were sampled 1-7 times daily from half the depth of the water column using a syringe headspace method (Borges et al. 2015) whereby four replicate syringes (Terumo, Japan), each fitted with a three-way stopcock, were used to equilibrate 30 ml of bubble-free sample water with 30 ml of N_2 gas. To reduce permeability to gas, each syringe was periodically coated with a thin film of petroleum jelly (Vaseline, Unilever). Replicate samples were equilibrated by shaking for 5-10 min and end-temperature measured with a mercury thermometer. The partial pressure of CO_2 in the equilibrated headspace gas was measured using an IRGA (LiCor LI-820), then converted to the fugacity of CO_2 (fCO_2) using:

$$fCO_2 = pCO_2 \cdot f(g) \quad (1)$$

where $f(g)$ is the fugacity coefficient (unitless; Millero 2007). The optical path of the IRGA was kept dry between measurements using a desiccant (Drierite). We then calculated $[CO_2^*]$ {i.e. the sum of $[CO_2]$ and $[H_2CO_3]$} according to Henry's Law:

$$[CO_2^*] = K_{0,CO2} \cdot fCO_2 \quad (2)$$

where $K_{0,CO2}$ is the CO_2 solubility constant at given temperature and salinity in mol L^{-1} atm^{-1} (Weiss 1974). The IRGA was calibrated using five gas standards ranging from zero to 18,100 ppm CO_2 in nitrogen (±2%). To correct for spatial and temporal thermal variability, CO_2 partial pressures reported herein were normalised to the mean daily water temperature of 11.8 °C. CH_4 was also sampled using the above-described syringe headspace method, whereby 240 ml of headspace gas from eight co-equilibrated syringes was transferred to an evacuated 0.5 L Tedlar bag (Restek, USA) and stored at 5 to 10 °C for transportation to the lab where analyses were performed on a calibrated Cavity Ring-down Spectrometer (G2201-*i*, Picarro, USA) within two hours of sampling. To account for variations of the range in aqueous O_2 and CO_2* concentrations occurring over a 24-hour time period, samples were collected at least two times per day for 50% of sampling days and included morning and evening sampling. Additional sampling was conducted to characterise natural diel fluctuations at the S1 site during conditions of disconnect, as well as shorter-term variability induced by rainfall. Where only one sample was collected per day samples were preferentially collected late morning to approximate the diel mean (Supplementary Table A2).

We present dissolved gas concentrations as excess CO_2, excess CH_4 and apparent oxygen utilization (AOU), being the deviation of each of these gases from atmospheric equilibrium (*x*eq; where *x* is the dissolved gas of interest; Richey et al. 1988):

$$\text{Excess } CO_2 = [CO_2^*] - [CO_2 eq] \quad (3)$$

208

209 $$\text{Excess } CH_4 = [CH_4] - [CH_4eq] \quad (4)$$

210

211 $$AOU = [O_2eq] - [O_2] \quad (5)$$

212

213 where $[O_2]$eq was calculated from dissolved oxygen % saturation measurements and

214 $[CO_2]$eq and $[CH_4]$eq were calculated from atmospheric samples collected *in-situ*, using

215 barometric pressure, temperature and salinity.

216

217 Chamber deployments and modelling

218

219 Water-air CO_2 fluxes were measured in duplicate on 10 occasions using a lightweight

220 static free-floating chamber (diameter, 300 mm; height, 140 mm; water column

221 penetration, 30 mm), integrated into a recirculating closed loop with the IRGA using a

222 microdiaphragm air pump (Parker, USA) and an inline desiccant (Drierite). Soil-to-air

223 CO_2 fluxes from the dry streambed were measured in duplicate on 11 occasions using a

224 second chamber (diameter, 150 mm; height, 100 mm), which was lowered onto a fixed

225 collar using the same closed-loop system. Chamber fluxes (F, mmol m^{-2} d^{-1}) were

226 calculated from the rate of change in chamber pCO_2 over time (Frankignoulle 1998):

227 $$F_{CO2} = \left(\frac{d(pCO2)}{dt}\right)\left(\frac{V}{RT_K S}\right) \quad (6)$$

228

where $d(pCO_2)/dt$ is the slope of the CO_2 accumulation inside the chamber (μatm s^{-1}), V is the chamber volume (L), T_K is ambient atmospheric temperature in degrees kelvin (K), S is the chamber surface area (m^2), and R is the universal gas constant (L atm K^{-1} mol^{-1}). Deployment durations were typically <5 min and observed increase of pCO_2 inside the chamber was linear for 97% of chamber measurements (r^2 = >0.95).

For background fluxes, we derived gas transfer velocities (k, in m d^{-1}) at the boundary layer interface from our floating chamber measurements, and converted k-CO_2 to k-CH_4 using temperature-dependent Schmidt numbers (Sc_T) suitable for freshwater (Jähne et al. 1987; Wanninkhof 2014):

$$k_{600} = k_{CO2} / (Sc_T /600)^{-n} \quad (7)$$

$$k_{CO2}/k_{CH4} = (Sc_{CO2}/Sc_{CH4})^{-n} \quad (8)$$

where n is the Schmidt number exponent depending on the condition of the aquatic boundary layer, which was set at 0.67 for lentic waters or 0.5 for flowing waters applying an arbitrary cut off value of a mean daily v of 0.1 m s^{-1}. We used the measured k-CO_2 and calculated k-CH_4 to estimate the flux for each gas according to:

$$F_{CO2} = k_{CO2} \cdot K_{0,CO2} (fCO_{2,water} - fCO_{2,air}) \quad (9)$$

$$F_{CH4} = k_{CH4} \cdot K_{0,CH4} (pCH_{4,water} - pCH_{4,air}) \quad (10)$$

where $CO_{2,water}$ /$CH_{4,water}$ and $CO_{2,air}$/$CH_{4,air}$ are the fugacity (f) or partial pressures (p) of each gas in the surface water and overlying atmosphere, respectively (Bakker et al. 2014), and $K_{0,CH4}$ is the CH_4 solubility according to the coefficients of Yamamoto et al. (1976).

Direct water-air flux measurements using floating chambers were excluded during hydrologic phase transitions as this method does not account for the influence of physical forcing by rainfall on the aquatic boundary layer and because anchored chambers tend to over-estimate fluxes in turbulent waters (Lorke et al. 2015). Thus, to account for the influence of rewetting events on k we also modelled our data empirically using two approaches, "HO" and "RAY", based on rainfall rate, Ho et al. (1997) and event-induced water velocity, Raymond et al. (2012), respectively:

$$k_{600}\,(\mathrm{HO}) = 0.929 + 0.679R_n - 0.0015R_n^2 \quad (11)$$

$$k_{600}\,(\mathrm{RAY}) = (vs)^{0.89} \cdot \mathrm{d}^{0.54} \cdot 5037 \quad (12)$$

where R_n is the rain rate (mm hr^{-1}), v is the water velocity (m s^{-1}), s is the slope of the study segment (unitless), and d is water depth (m).

Statistical analyses and hydrologic delineations

For statistical analyses of C-gas species with environmental and morphological variables we used Pearson's least square regression for linear covariance (StatPlus, AnalystSoft Inc.), with significance herein implied at the 95% confidence interval ($p<0.05$). Wet and

dry cycles at the S1 study site were delineated using a water-to-soil ratio of 0.5, which coincided with a daily mean stage height of 0.0 m.

Results

Stream morphometry and ancillary variables

Throughout the 56-day sampling period stream depth, width and volume at the primary S1 study segment ranged from to 0.0 to 0.3 m, 0.0 to 1.4 m and 0.0 to 7.1 m^3. The minimum depth of the water table below the level of the streambed was -0.23 m occurring on the final day of the second, longer dry-cycle. pH ranged from 4.57 to 7.15 and was typically neutral during rainfall trending to acidic post-stormflow, exhibiting a significant negative relationship with [CO_2*] ($r^2 = 0.78$, $n = 26$, $p < 0.05$). The measured ambient atmospheric and water temperatures ranged from 2.0 to 30.9 °C and 3.9 to 20.4 °C, with maximum 36-hour range in variability of up to 23.1 and 9.8 °C, respectively. Rainfall intensity ranged from 0.0 to 77.8 mm hr^{-1} with a daily mean of 0.7 ± 0.9 mm hr^{-1} (± SD herein) (Supplementary Table A1 and A2).

Dissolved gas concentrations and net fluxes

In-situ water column excess CO_2 at the upstream S1 timeseries station fluctuated over two orders of magnitude from -11 to 1600 μM (289 to 30,800 μatm pCO_2), with a daily mean of 756 ± 427 μM (15,300 ± 8380 μatm; Fig. 2). Concentrations decreased towards atmospheric equilibrium during stormflow. Undersaturation was evident only during a

299 hailstorm event that occurred at the onset of the initial wet-cycle, coinciding with the
300 temperature-dependent CO_2 solubility maxima (0.067 mol L^{-1} atm^{-1}). The diel evolution
301 of dissolved oxygen concentrations with respect to atmospheric equilibrium increased
302 over the duration the wet cycles, with AOU ranging from -177 to 323 μM (daily mean,
303 106 ± 86 μM; Fig. 2 and Fig. 3). Daily $\Delta[CO_2]$ was consistently greater than $\Delta[O_2]$ by a
304 factor of 1.5 to 4.7, with both variables exhibiting a linear increase over time throughout
305 the initial, longer wet-cycle (r^2 = 0.84 and 0.87, respectively, n = 12, $p < 0.05$; Fig. 4)
306 indicating net production of CO_2 via both in-stream processes and hyporheic exchange.
307 Over the two days of spatial sampling between-site variability in excess CO_2
308 within the 100 m study segment ranged up to 1200 μM (23,900 μatm; with samples
309 collected at the same stage height and time of day). The highest excess CO_2
310 concentrations occurred at the S3 station, situated at the inlet of the man-made peat
311 swamp channel at 1390 ± 227 μM (28,400 ± 4720 μatm; Table 1). The less-frequently
312 inundated upstream sites with vegetation exhibited the greatest excess CO_2 variability
313 between wet-cycles (S1 and S2, 700 and 550 μM, respectively), whereas the more-
314 frequently inundated downstream sites that were void of vegetation were least variable
315 (S3-S5, 322, 86 and 45 μM, respectively).
316 Excluding the influence of rainfall-induced turbulence and based on temporal
317 changes in concentrations alone, the measured instantaneous diffusive water-air CO_2-C
318 fluxes ranged from 11 to 80 mmol m^{-2} d^{-1} (mean, 45 ± 28 mmol m^{-2} d^{-1}; n = 6).
319 Measurements of the gas transfer velocity (k_{600}) averaged 0.26 ± 0.10 m d^{-1}, decreasing 2-
320 fold at the S1 timeseries station during the initial wet-cycle from 0.33 to 0.16 m d^{-1}.
321 Applying the average k-value obtained from all chamber measurements, instantaneous

322 diffusive water-air CO_2-C fluxes ranged from -1 to 78 mmol m^{-2} d^{-1} (mean, 37 ± 21 mmol
323 m^{-2} d^{-1}; n = 59; Fig. 5). The measured instantaneous inter-site spatial variability in water-
324 air CO_2-C fluxes ranged up to 76 mmol m^{-2} d^{-1}, being similar in magnitude to the *in-situ*
325 temporal variability observed at the S1 timeseries station.

326 The influence of rainfall on k and CO_2-C fluxes during hydrologic transitions was
327 calculated in this study via empirical equations. Considering only occasions influenced
328 by precipitation >1 mm (n = 9 days), instantaneous k_{600} (HO) values ranged from 0.22 to
329 10.72 m d^{-1}, with a daily mean of 0.38 ± 0.17 m d^{-1}. Corresponding CO_2-C fluxes ranged
330 from 0 to 567 mmol m^{-2} d^{-1}, with a daily mean of 26 ± 23 mmol m^{-2} d^{-1}. Considering only
331 occasions with flow velocities ≥0.05 m s^{-1} (n = 9 days), the slope-velocity
332 parameterisation of Raymond et al. (2012) produced k_{600} values ranging from 0.27 to 1.40
333 m d^{-1}, with a daily mean of 0.53 ± 0.39 m d^{-1}. The corresponding CO_2-C fluxes on these
334 occasions ranged from -3 to 173 mmol m^{-2} d^{-1}, with a daily mean of 67 ± 38 mmol m^{-2} d^{-1}
335 (Fig. 5; Supplementary Table A3). The influences of boundary layer condition on gas
336 transfer velocities from both direct (e.g., physical forcing) and indirect disturbance (e.g.,
337 changes to stream turbulence) may be approximately linearly additive, as with rainfall
338 and wind speed (Ho et al. 2007). Under this assumption, the mean daily evasion rate
339 during rainfall-induced hydrologic transitions was ~2 times higher than the mean
340 background flux rate determined using floating chambers during still waters (59 ± 46 and
341 33 ± 24 mmol m^{-2} d^{-1}, respectively).
342
343 Integrated water- and soil-air fluxes
344

345 The measured daily mean CO_2-C evasion rate from dry portions of the streambed was 72
346 ± 27 mmol m^{-2} d^{-1} (range, 27 to 115 mmol m^{-2} d^{-1}), and was ~20% higher than the
347 calculated mean daily water-air evasion rate encompassing changes from lotic to lentic
348 waters. The peak-measured soil-air efflux occurred four-days after the onset of the
349 second, longer dry-cycle when the mean stage height was -0.06 m. Factored for temporal
350 changes to the water/soil ratio, the [CO_2*] saturation status, and water-air boundary layer
351 condition over time the integrated daily mean flux of CO_2-C from the S1 study segment
352 was 61 ± 24 mmol m^{-2} d^{-1} (range, 12 to 156 mmol m^{-2} d^{-1}; Fig. 5). This analysis employs
353 the mean soil CO_2 flux obtained from all measurements to fill data gaps, thus assuming
354 inhomogeneity throughout the streambed with progressive drying due to variable
355 negative stage height and subsurface oxygen dynamics, and, that the mean soil CO_2 flux
356 rate represents the average of all partial fluxes.
357
358 Water column excess CH_4 and net fluxes
359
360 Excess CH_4 increased from 0.6 to 14.6 μM (349 to 8700 μatm pCH_4) at the S1 station
361 over the initial wet-cycle, with a median concentration of 2.1 μM (1200 μatm) and
362 median calculated background CH_4-C evasion rate of 0.3 mmol m^{-2} d^{-1} (range, 0.1 to 1.9
363 mmol m^{-2} d^{-1}). The maximum water column CH_4 concentrations occurred towards the
364 end of the initial, longer wet-cycle (Fig. 2). Spatial variability in excess CH_4 ranged from
365 0.4 to 12.9 μM (239 to 7940 μatm), with resultant background water-air CH_4-C evasion
366 rates ranging from 0.1 to 1.7 mmol m^{-2} d^{-1} (overall mean, 0.7 ± 0.6 mmol m^{-2} d^{-1}).
367

368 Wet and dry cycle dynamics

369

370 A decrease in wet-cycle duration (T_W) coincided with a decrease in daily mean water
371 column excess CO_2 concentrations (wet-cycle 1-3, 949 ± 322, 298 ± 203 and 213 ± 155
372 μM; T_W = 19, 5 and 2 d, respectively, $r^2 = 0.99$, $p < 0.05$; Fig. 6a) and integrated water and
373 soil-air CO_2-C evasion rates (wet-cycle 1-3, 65 ± 32, 30 ± 10, and 21 ± 14 mmol m^{-2} d^{-1},
374 respectively; Fig. 6b). Stage height correlated significantly with daily evapotranspiration
375 rate ($r^2 = 0.49$, $n = 56$, $p < 0.05$), daily $\Delta[CO_2]$ and $\Delta[O_2]$ (wet-cycle 1, $r^2 = 0.73$ and
376 0.77, respectively, $n = 12$, $p < 0.05$), water/soil ratio-corrected fluxes (water, $r^2 = 0.52$;
377 soil, $r^2 = 0.93$; $p < 0.05$; Fig. 7), as well as with water temperature ($r^2 = 0.23$; $p < 0.05$).

378

379 **Discussion**

380

381 Water-air versus soil-air exchange

382

383 Our results from an intermittent stream supports recent research from seasonally
384 ephemeral aquatic systems which show that mean soil-air CO_2-C fluxes typically exceed
385 those from the same watercourses when inundated (Table 2). Based on *in-situ*
386 measurements when the stream study sites were disconnected, the contributions of soil-
387 air CO_2-C fluxes at the S1 timeseries station exceeded water-air fluxes by a factor of ~2.
388 However, this does not account for changes to the emerged/submerged area over time, or
389 to stream flow dynamics during dry-to-wet and baseflow-stormflow hydrologic
390 transitions. In the case of the upper Jamison Creek watercourse, integrating these factors

391 into the analyses produced contrasting results; with the contributions of water- and soil-
392 air evasion to total CO_2-C fluxes being approximately equal (43 and 40 mol,
393 respectively).

394 System-specific dissimilarities in wet and dry cycle intermittence in this study
395 influenced areal water-soil distributions, spatial flux dynamics, and, consequently, the
396 relative magnitude of total C-gas fluxes. Further, antecedent soil moisture conditions
397 linked to the length of the preceding dry-cycle and consequent negative stage height
398 influences the duration of each rewetting-cycle (Mohanty et al. 2015) and nutrient
399 hydrochemistry (Biron et al. 1999), in conjunction with prevailing meteorological
400 conditions (e.g. rain event intensity and duration; percent cloud cover). Considering this,
401 we hypothesize that GHG fluxes in frequently intermittent watercourses are likely to
402 display contrasting characteristics to seasonally ephemeral watercourses over annual time
403 scales. Accordingly, it may prove more accurate to apply a distinction between the wet
404 and dry fraction periods of seasonally ephemeral watercourses (typically dry for months
405 at a time) and other more frequently intermittent aquatic systems (wet and dry cycles
406 ranging from days to weeks) for the future integration of non-perennial fluvial systems
407 into global carbon budget models.

408 The rates of GHG evasion from low-order streams can be disproportionately high
409 in magnitude compared to other fluvial systems of the lower catchment, with a general
410 trend of decreasing gas transfer velocities and pCO_2 with increasing stream order
411 (Butman and Raymond 2011). For example, in a paraglacial mixed forest watershed
412 (Québec, Canada), the smallest first-order streams represented <20% of the total river
413 network surface and contributed >35% of the total fluvial GHG emissions (Campeau et

al. 2014). The CO_2 evasion rates reported for an intermittent watercourse in this study and reported for both wet and dry cycles in seasonally ephemeral watercourses in semi-arid environments (von Schiller et al. 2014; Gómez-Gener et al. 2016), are typically lower than evasion rates reported for perennial flowing waters (Butman and Raymond 2011; Raymond et al. 2013) and are more similar to evasion rates reported for still waters (Raymond et al. 2013; Catalán et al. 2014; Weyhenmeyer et al. 2015; Holgerson 2016) and wetlands (Sonnentag et al. 2010; Sjögersten et al. 2014) (Table 2).

'Hot' and 'cold' phenomena in C-gas evasion cycle

Spatial and temporal patterns in stream hydrologic status alter biotic assemblage composition and ecosystem metabolism (Hall et al. 2015; Sabater et al. 2016), nutrient biogeochemistry (Birch 1958; Mohanty et al. 2015), soil diffusivity (Davidson and Janssens 2006), benthic redox dynamics (Harrison et al. 2005; Knorr et al. 2009; Gallo et al. 2014), as well as dissolved organic matter composition and lability (Buffam et al. 2001; Raymond and Saiers 2010; Jeanneau et al. 2015). Such changes can drive spatially variable 'hot' and 'cold' moments in the dry-wet-dry C-gas evasion cycle (i.e., increased and decreased fluxes, respectively; McClain et al. 2003). For example, in urbanized ephemeral waterways in Arizona, USA Gallo et al. (2014) found CO_2-C emissions to increase following temporary rewetting of the dry streambed sediments (soil moisture content $\leq$18$\pm$3% and t $\leq$6-hours; pre-wetting, 65 $\pm$ 53 mmol m^{-2} d^{-1}; post-wetting peak, 706 $\pm$ 453 mmol m^{-2} d^{-1}; sandy-loam soil group); with the flux magnitude correlated to soil moisture status. Our soil chamber measurements did not detect a notable increase in

dry-cycle soil fluxes following partial rewetting. However, the empirical modelling presented herein considering complete cycles of inundation and emersion (e.g., stage height during rewetting >0 m; T_W = >1 d), demonstrated that intense physical forcing by transient meteorological events can also produce further hydrologically mediated 'hot moment' phenomena during which water-air fluxes can equal or exceed soil fluxes.

Of the two models used to calculate the influence of environmental variables on the rates of water-air CO_2-C fluxes, we found the parameterisation given by Ho et al. (1997) to closely approximate the mean background water column gas transfer velocities as determined from floating chamber measurements (when R_n = 0.00 mm hr^{-1}, k_{600} (HO) = 0.22 m d^{-1}; mean chamber-derived k_{600} in this study, 0.26 ± 0.10 m d^{-1}). The Ho et al. (1997) model was developed using sulphur hexafluoride (SF_6) tracer injections in a closed system and incorporated the kinematic energy flux of natural raindrop size distributions, which monotonically decreases as raindrop size decreases (Marshall and Palmer 1948). Incorporating the influence of physical forcing by precipitation at the water-air boundary layer during hydrologic phase transitions, this parameterisation increases our mean daily background fluxes of CO_2-C on days influenced by rainfall by 30%, with the maximum instantaneous evasion rate of 567 mmol m^{-2} d^{-1} being 5 times higher than our measured peak post-wet-cycle soil flux rate of 115 mmol m^{-2} d^{-1}.

The effect of precipitation on evasion is most pronounced where wind velocity does not dominate turbulence-driven C-gas exchange in limnological systems such as small ponds (Ho et al. 1997; Vachon and Prairie 2013). In this study, hydrophobic macromolecular surfactants (personal observations) may have diminished the kinematic energy flux produced by boundary layer raindrop penetration (e.g. Frew et al. 1990,

460 2004; McKenna and McGillis 2004), as evidenced by the 47% decrease in measured k_{600}
461 over the initial wet-cycle. As time progresses since rewetting, so does the thickness and
462 extent of surfactants. This in turn limits the transfer of gases, reducing water column
463 reaeration capacity and engendering an accumulation of CO_2 (e.g., Fig. 6a). Importantly,
464 the presence of surfactants would most likely inhibit C-gas evasion rates during
465 precipitation events that occur throughout the later term of a phytoplankton-dominated
466 wet-cycle, prior to flushing of the system by significant rainfall.

467 Under low-flow conditions, the slope-depth-velocity parameterisation of
468 Raymond et al. (2012) also provided a reasonable approximation of the gas transfer
469 velocities determined from our chamber measurements (mean k_{600} difference, ± 0.1 m d^{-1}
470). This model was formulated from 563 purposeful tracer experiments in running waters
471 of varying stream order and flow conditions. Overall, k_{600} (RAY) was 2.1 times greater
472 than our measured gas transfer velocities, with the discrepancy between measured and
473 modelled k_{600} being due to the exclusion of higher flow velocities by our chamber
474 measurements (e.g. because of inherent limitations of using floating chambers to
475 determine k in running waters; Kremer et al. 2003; Lorke et al. 2015). Inclusive of the
476 influence of stream hydraulics, this parameterisation increases our mean daily
477 background CO_2-C fluxes on occasions with flow velocities >0.05 m s^{-1} by 60%, with a
478 maximum increase of 108 mmol m^{-2} d^{-1} (163%) on the first day of the initial wet-cycle
479 post-rainfall, coinciding with a subsidence in stormflow and concurrent increase in excess
480 CO_2 concentrations.

481 For both measured and modelled fluxes, CO_2 degassing from the S1 segment
482 ceased during periods of heavy rainfall when aqueous [CO_2*] approached atmospheric

equilibrium, as well as during the initial hailstorm event when there was a short two-hour period of net influx of CO_2 due to rapid cooling of the water and a subsequent increase in CO_2 solubility. During storm events, such equilibrium and undersaturation states in typically supersaturated aquatic systems may also be preceded by a pulse of elevated CO_2 degassing relative to baseflow rates (Looman et al. 2016), as increased streamwater velocity increases the gas transfer velocity due to higher streambed-generated shear stress (Beaulieu et al. 2012). The precipitation-induced dilution effect may then be succeeded by an increase in water column [CO_2*] derived from soil respiration, transported by the migration of surface waters infiltrating through groundwater pathways (Johnson et al. 2007, 2008; Dinsmore et al. 2013). Thus, the combined influence on water-air gas exchange rates of rainfall induced changes in gas transfer velocity as well as CO_2* concentration-discharge hysteresis patterns is temporally erratic.

Overall, dry-to-wet and baseflow-stormflow hydrological transitions represented 25% of wet-cycle days yet contributed 42% of total water-air CO_2-C emissions. Evasion rates were lowest on rewetting days with precipitation >10 mm, with such cold moments decreasing fluxes by up to 100% with respect to mean non-transition phase water-air fluxes (average decrease of 20%). Conversely, fluxes were increased by and average of 12% on days with precipitation ranging from 1 to 10 mm and by 20% on days with precipitation <1 mm. Regarding the latter, this increase is primarily attributable to residual post-rainfall flow velocities of up to 0.1 m s^{-1} compared to those fluxes occurring in otherwise still waters. Accordingly, the maximal water-air CO_2 flux potential in the present study occurred as a result of short-term physical forcing by rainfall when the streambed was previously inundated and not necessarily during peak partial pressures as

might otherwise be expected. Importantly, the degree of misinterpretation for total water-air CO_2 flux accounting if non-continuous sampling methods are employed would be site-specific, and would be largely dependent upon the pCO_2 status; the frequency, duration and magnitude of rainfall events; relative changes to the streambed water/soil ratio during hydrologic phase transitions; and, moreover, the timing and frequency that periodic samples are taken. We highlight that additional studies are required for these findings to be generalised to other catchments.

The contribution of methane

The sustained global warming potential (SGWP; Neubauer and Megonigal 2015) of mean daily water-air CH_4 contributions to total C-gas emissions from the S1 study segment - expressed as CO_2 equivalents - were similar to the SGWPs of mean soil CO_2 emissions over a 20-year time frame and to measured background water-air emissions over a 100-year time frame (76 ± 67 and 36 ± 25 mmol m^{-2} d^{-1} CO_2 equivalents, respectively). As we only considered diffusive CH_4 fluxes in this study, additional contributions via the ebullition pathway (e.g., Prairie and del Giorgio 2013) would likely extend the contributions of CH_4 fluxes to total C-gas emissions from the S1 study segment to beyond those of CO_2 from both the soil- and water-air interfaces over the 20 and 100-year time frames, respectively.

The maximum water column excess CH_4 concentrations in the present study occurred during the final time period of the initial 21-day wet-cycle (Fig. 2), akin to the observed trends in CO_2. Low nocturnal dissolved oxygen saturations that occurred post-

529 wetting (25 ± 6% saturation) might have facilitated anaerobic metabolism and methane
530 production. The hyporheic zone of the streambed represents the interface between ground
531 and surface waters and is a dynamic ecotone for microbial metabolism (Claret and
532 Boulton 2009), with the degradation of organic matter in surface sediments causing
533 localised oxygen depletions. As well as the traditional pathway of microbial anaerobic
534 methanogenesis, CH_4 production can also occur in oxic waters via acetoclastic
535 methanogenesis, driven by algal dynamics (Bogard et al. 2014). CO_2 can be produced in
536 turn by the oxidation of methane, both aerobically and anaerobically (Thauer et al. 2008).
537 Thus, although stoichiometric analyses of the biogeochemical drivers of CH_4 dynamics
538 were beyond the specific aims of the present study the temporal changes for trends in
539 AOU and excess CO_2, as well as a significant negative relationship between excess CH_4
540 and $[H^+]$ ($r^2 = 0.78$; $p < 0.05$), suggest that successions in microbial and algal community
541 composition may be responsible for an increase in CH_4 production over longer-duration
542 wet-cycles. Such potential competitive exclusion processes most likely occur in
543 conjunction with post-rewetting redox oscillations of oxidised iron and sulphate substrate
544 available for anaerobic metabolism (Knorr et al. 2009). Additionally, correlations
545 between excess CH_4 and both ambient atmospheric and water temperatures ($r^2 = 0.67$ and
546 0.31, respectively, $p < 0.05$) and water temperature with CH_4:CO_2 ratio ($r^2 = 0.83$; $p <$
547 0.05) indicate that methanogenesis may be temperature dependent over short time scales,
548 and reflect the physiological kinetic processes generating these fluxes (see Yvon-
549 Durocher et al. 2014).
550
551 **Conclusions and implications**

552

553 Our observations demonstrate that wet and dry cycle periodicity, redox processes,
554 atmospheric forcing by rainfall, site-specific ephemerality, and small-scale spatial
555 heterogeneity were key influential factors in controlling C-gas flux rates in the upper
556 Jamison Creek watercourse. In non-perennial watercourses maximal and minimal fluxes
557 may occur during hydrologic phase transitions, and, although short-lived and problematic
558 to quantify at larger regional scales such hot and cold moments may comprise an
559 appreciable component of the local and regional carbon budgets for aquatic systems. Up
560 to 75% of watercourses in Australia are ephemeral (Sheldon et al. 2010) and these non-
561 perennial watercourses are currently excluded from Australia's carbon accounting
562 estimates (Haverd et al. 2013; Poulter et al. 2014). Therefore, due to the high rate of
563 emissions from dry watercourses, as well as fluctuant nature in the rate of emissions
564 during and following complete or partial rewetting, the overall relative magnitude of this
565 continental carbon sink and that of other semi-arid ecosystems of the southern
566 hemisphere may be misrepresented.

567

568 **Conflict of interest**

569 The authors declare that they have no conflict of interest.

References

Alin SR, Rasera MF, Salimon CI, Richey EJ, Holtgrieve GW, Krusche AV, Snidvongs A (2011) Physical controls on carbon dioxide transfer velocity and flux in low-gradient river systems and implications for regional carbon budgets. J Geophys Res 116:G01009

Bakker DC, Bange HW, Gruber N (2014) Air-sea interactions of natural long-lived greenhouse gases (CO_2, N_2O, CH_4) in a Changing Climate. In Ocean-Atmosphere Interactions of Gases and Particles, Liss PS, Johnson MT (eds). Springer Earth System Sciences

Bass AM, Munksgaard NC, Leblanc M, Tweed S, Bird MI (2014) Contrasting carbon export dynamics of human impacted and pristine tropical catchments in response to a short-lived discharge event. Hydrol Process 28:1835–1843

Battin TJ, Luyssaert S, Kaplan LA, Aufdenkampe AK, Richter A, Tranvik LJ (2009) The boundless carbon cycle. Nat Geosci 2:598–600

Beaulieu JJ, Shuster WD, Rebholz JA (2012) Controls on gas transfer velocities in a large river. J Geophys Res Biogeosci 117:G02007

Bernal S, Schiller D, Sabater F, Martí E (2012) Hydrological extremes modulate nutrient dynamics in Mediterranean climate streams across different spatial scales. Hydrobiologia 719:31–42

Bernot MJ, Sobota DJ, Hall RO et al (2010) Inter-regional comparison of land-use effects on stream metabolism. Freshwater Biol 55:1874–1890

Birch HF (1958) The effect of soil drying on humus decomposition and nitrogen availability. Plant and Soil 10:9–31

Biron PM, Roy AG, Courschesne F, Hendershot WH, Côté B, Fyles J (1999) The effects of antecedent moisture conditions on the relationship of hydrology to hydrochemistry in a small forested watershed. Hydrol. Process. 13:1541–1555

Bogard MJ, del Giorgio PA, Boutet L et al (2014) Oxic water column methanogenesis as a major component of aquatic CH_4 fluxes. Nature Communications 5:5350

Borges AV, Darchambeau F, Teodoru CR et al (2015) Globally significant greenhouse-gas emissions from African inland waters. Nat Geosci 8:637–642

Buffam I, Galloway JN, Blum LK, McGlathery KJ (2001) A stormflow/baseflow comparison of dissolved organic matter concentrations and bioavailability in an Appalachian stream. Biogeochemistry 53:269–306.

Bureau of Meteorology (BoM) (2015a) Climate Data Online. Australian Government Bureau of Meteorology. http://www.bom.gov.au/climate/averages/tables/cw_063039.shtml. Accessed 26 October 2015

Bureau of Meteorology (BoM) (2015b) Climate Data Online. Australian Government Bureau of Meteorology. http://www.bom.gov.au/watl/eto/. Accessed 26 October 2015

Butman D, Raymond PA (2011) Significant efflux of carbon dioxide from streams and rivers in the United States. Nat Geosci 4:839–842

Campeau A, Lapierre J, Vachon D, del Giorgio PA (2014) Regional contribution of CO_2 and CH_4 fluxes from the fluvial network in a lowland boreal landscape of Québec. Global Biogeochem Cy 28:1–13

Casas-Ruiz JP, Tittel J, von Schiller D (2016) Drought-induced discontinuities in the source and degradation of dissolved organic matter in a Mediterranean river. Biogeochemistry 127:125–139

Catalán N, von Schiller D, Marcé R, Koschorreck M, Gómez-Gener L, Obrador B (2014) Carbon dioxide efflux during the flooding phase of temporary ponds. Limnetica 33:349–360

Claret C, Boulton A (2009) Integrating hydraulic conductivity with biogeochemical gradients and microbial activity along river–groundwater exchange zones in a subtropical stream. Hydrogeol J 17:151–160

Costigan KH, Daniels MD, Dodds WK (2015) Fundamental spatial and temporal disconnections in the hydrology of an intermittent prairie headwater network. J Hydrol 522:305–316

Crusius J, Wanninkhof R (2003) Gas transfer velocities measured at low wind speed over a lake. Limnol Oceanogr 48:1010–1017

Datry T, Larned ST, Tockner K (2014) Intermittent rivers: a challenge for freshwater ecology. Bioscience 64:229–235

Davidson EA Janssens IA (2006) Temperature sensitivity of soil carbon decomposition and feedbacks to climate change. Nature 440:165–73

Dieter D, von Schiller D, García-Roger EM, et al (2011) Preconditioning effects of intermittent stream flow on leaf litter decomposition. Aquat Sci 73:599–609

Dinsmore KJ, Billett MF (2008) Continuous measurement and modeling of CO_2 losses from a peatland stream during stormflow events. Water Resour Res 44:W12417

Dinsmore KJ, Wallin MB, Johnson MS, Billett MF, Bishop K, Pumpanen J, Ojala A (2013) Contrasting CO_2 concentration discharge dynamics in headwater streams: a multi-catchment comparison. J Geophys Res Biogeosci 118: 445–461

Dodds WK (2006) Eutrophication and trophic state in rivers and streams. Limnol Oceanogr 51:671–680

Dodds WK, Perkin JS, Gerken JE (2013) Human impact on freshwater ecosystem services: a global perspective. Environ Sci Technol 47:9061−9068

Fazi S, Vazquez E, Casamayor EO, Amalfitano S, Butturini A (2013) Stream hydrological fragmentation drives bacterioplankton community composition. PLoS ONE 8:e64109

Frankignoulle M (1988) Field measurements of air-sea CO_2 exchange. Limnol Oceanogr 33:313–322

672 Frew NM, Bock EJ, Schimpf U et al (2004) Air-sea gas transfer: its dependence on wind stress,
673 small-scale roughness, and surface films. J Geophys Res 109:C08S17
674
675 Frew NM, Goldman JC, Dennett MR, Johnson AS (1990) Impact of phytoplankton-generated
676 surfactants on air-sea gas exchange. J Geophys Res 95:3337–3352
677
678 Fryirs KA, Cowley K, Hose GC (2016) Intrinsic and extrinsic controls on the geomorphic
679 condition of upland swamps in Eastern NSW. Catena 137:100–112
680
681 Gallo EL, Lohse KA, Ferlin CM et al (2014) Physical and biological controls on trace gas fluxes
682 in semi-arid urban ephemeral waterways. Biogeochemistry 121:189–207
683
684 Godsey SE, Kirchner JW (2014) Dynamic, discontinuous stream networks: hydrologically driven
685 variations in active drainage density, flowing channels and stream order. Hydrol Process
686 28:5791–5803
687
688 Gómez-Gener L, Obrador B, Marcé R et al (2016) When water vanishes: magnitude and
689 regulation of carbon dioxide emissions from dry temporary streams. Ecosystems 19:710–723
690
691 Hagen EM, McTammany ME, Webster JR, Benfield EF (2010) Shifts in allochthonous input and
692 autochthonous production in streams along an agricultural land-use gradient. Hydrobiologia
693 655:61–77
694
695 Haines AT, Finlayson BL, McMahon TA (1988) A global classification of river regimes. Appl
696 Geogr 8:255–272
697
698 Hall RO, Yackulic CB, Kennedy TA et al (2015) Turbidity, light, temperature, and hydropeaking
699 control primary productivity in the Colorado River, Grand Canyon. Limnol Oceanogr 60:512–
700 526
701
702 Hansen WF (2001) Identifying stream types and management implications. Forest Ecol Manag
703 143:39–46
704
705 Harrison JA, Matson PA, Fendorf SE (2005) Effects of a diel oxygen cycle on nitrogen
706 transformations and greenhouse gas emissions in a eutrophied subtropical stream. Aquat Sci
707 67:308–315
708
709 Haverd V, Raupach MR, Briggs PR et al (2013) The Australian terrestrial carbon budget.
710 Biogeosciences 10:851–869
711
712 Ho DT, Bliven LF, Wanninkhof R, Schlosser P (1997) The effect of rain on air-water gas
713 exchange. Tellus B 49:149–158
714
715 Ho DT, Veron F, Harrison E, Bliven LF, Scott N, McGillis WR (2007) The combined effect of
716 rain and wind on air–water gas exchange: a feasibility study. J Marine Syst 66:150–160
717
718 Holgerson MA, Raymond PA (2016) Large contribution to inland water CO_2 and CH_4 emissions
719 from very small ponds. Nat Geosci 9:222–226
720
721 Holmes NT (1999) Recovery of headwater stream flora following the 1989–1992 groundwater
722 drought. Hydrol Process 13:341–54

Hook AM, Yeakley JA (2005) Stormflow dynamics of dissolved organic carbon and total dissolved nitrogen in a small urban watershed. Biogeochemistry 75:409–431

Jähne B, Münnich K, Dutzi R, Huber W, Libner P (1987) On the parameters influencing air‐water gas exchange. J Geophys Res 92:1937‐1949

Janke BD, Finlay JC, Hobbie SE, Baker LA, Sterner RW, Nidzgorski D, Wilson BN (2014) Contrasting influences of stormflow and baseflow pathways on nitrogen and phosphorus export from an urban watershed. Biogeochemistry 121:209–228

Jeanneau L, Denis M, Pierson-Wickmann A, Gruau1 G, Lambert T, Petitjean P (2015) Sources of dissolved organic matter during storm and inter-storm conditions in a lowland headwater catchment: constraints from high-frequency molecular data. Biogeosciences 12:4333–4343

Johnson MS, Lehmann J, Riha SJ, Krusche AV, Richey JE, Ometto JP, Couto EG (2008) CO_2 efflux from Amazonian headwater streams represents a significant fate for deep soil respiration. Geophys Res Lett 35:L17401

Johnson MS, Weiler M, Couto EG, Riha SJ, Lehmann J (2007) Storm pulses of dissolved CO_2 in a forested headwater Amazonian stream explored using hydrograph separation. Water Resour Res 43:W11201

Jones JB, Mulholland PJ (1998) Carbon dioxide variation in a hardwood forest stream: an integrative measure of whole catchment soil respiration. Ecosystems 1:183–196

Knorr KH, Lischeid G, Blodau C (2009) Dynamics of redox processes in a minerotrophic fen exposed to a water table manipulation. Geoderma 153:379–392

Kremer J, Nixon S, Buckley B, Roques P (2003) Technical note: conditions for using the floating chamber method to estimate air–water gas ex- change. Estuar Coast 26:985–990

Koprivnjak JF, Dillon PJ, Molot LA (2010) Importance of CO_2 evasion from small boreal streams. Global Biogeochem Cy 24:GB4003

Larned ST, Datry T, Arscott DB, Tockner K (2010) Emerging concepts in temporary-river ecology. Freshwater Biol 55:717–38

Leopold LB, Maddock T (1953) The hydraulic geometry of stream channels and some physiographic implications. United States Geological Survey 1–57

Looman A, Santos IR, Tait DR, Webb JR, Sullivan CA, Maher DT (2016) Carbon cycling and exports over diel and flood-recovery timescales in a subtropical rainforest headwater stream. Sci Total Environ 550:645–657

Lorke A, Bodmer P, Noss C et al (2015) Technical note: drifting versus anchored flux chambers for measuring greenhouse gas emissions from running waters. Biogeosciences 12:7013–7024

Marshall JS, Palmer WM (1948) The distribution of raindrops with size. J Meteorol 5:165-166

McClain ME, Boyer EW, Dent CL et al (2003) Biogeochemical hot spots and hot moments at the interface of terrestrial and aquatic ecosystems. Ecosystems 6:301–312

McKenna SP, McGillis WR (2004) The role of free-surface turbulence and surfactants in air–water gas transfer. Int J Heat Mass Tran 47:539–553

McMahon TA, Finlayson BL (2003) Droughts and anti-droughts: the low flow hydrology of Australian rivers. Freshwater Biol 48:1147–1160

Millero FJ (2007) The marine inorganic carbon cycle. Chem Rev 107:308−341

Mohanty SK, Saiers JE, Ryan JN (2015) Colloid mobilization in a fractured soil during dry−wet cycles: role of drying duration and flow path permeability. Environ Sci Technol 49:9100−9106

Nadeau TL, Rains MC (2007) Hydrological connectivity between headwater streams and downstream waters: how science can inform policy. J Am Water Resour Assoc 43:118–133

Neubauer SC, Megonigal JP (2015) Moving beyond global warming potentials to quantify the climatic role of ecosystems. Ecosystems 18:1000–1013

Palta MM, Ehrenfeld JG, Groffman PM (2014) ‘‘Hotspots’’ and ‘‘Hot Moments’’ of Denitrification in Urban Brownfield Wetlands. Ecosystems 17: 1121–1137

Peter H, Singer GA, Preiler C, Chifflard P, Steniczka G, Battin TJ (2014) Scales and drivers of temporal pCO_2 dynamics in an Alpine stream. J Geophys Res Biogeosci 119:1078–1091

Poulter B, Frank D, Ciais P et al (2014) Contribution of semi-arid ecosystems to interannual variability of the global carbon cycle. Nature 509:600–603

Prairie YT, del Giorgio PA (2013) A new pathway of freshwater methane emissions and the putative importance of microbubbles. Inland Waters 3:311–320

Raymond PA, Hartmann J, Lauerwald R et al (2013) Global carbon dioxide emissions from inland waters. Nature 503:355–359

Raymond PA, Saiers JE (2010) Event controlled DOC export from forested watersheds. Biogeochemistry 100:197–209

Raymond PA, Zappa CJ, Butman D et al (2012) Scaling the gas transfer velocity and hydraulic geometry in streams and small rivers. Limnol Oceanogr–Fluids Environ 2:41–53

Raymond PA, Saiers JE, Sobczac WV (2016) Hydrological and biogeochemical controls on watershed dissolved organic matter transport: pulse-shunt concept Ecology 97(1): 5–16

Regnier P, Friedlingstein P, Ciais P et al (2013) Anthropogenic perturbation of the carbon fluxes from land to ocean. Nat Geosci 6:597–607

Richey JE, Devol AH, Wofsy SC, Victoria R, Riberio MN (1988) Biogenic gases and the oxidation and reduction of carbon in Amazon River and floodplain waters. Limnol Oceanogr 33:551–561

Ruiz-Halpern S, Maher DT, Santos IR, Eyre BD (2015) High CO_2 evasion during floods in an Australian subtropical estuary downstream from a modified acidic floodplain wetland. Limnol Oceanogr 60:42–56

Rudorff CM, Melack JM, MacIntyre S, Barbosa CC, Novo EM (2011) Seasonal and spatial variability of CO_2 emission from a large floodplain lake in the lower Amazon. J Geophys Res 116:G04007

Sabater S, Timoner X, Borrego C Acuña V (2016) Stream biofilm responses to flow intermittency: from cells to ecosystems. Frontiers in Environmental Science 4:14. doi:10.3389/fenvs.2016.00014

Sadat-Noori M, Maher DT, Santos IR (2015) Groundwater discharge as a source of dissolved carbon and greenhouse gases in a subtropical estuary. Estuar Coast 39:639-656

Salemi LF, Groppo JD, Trevisan R, de Moraes JM, de Paula Lima W, Martinelli LA (2012) Riparian vegetation and water yield: a synthesis. J Hydrol 454–455:195–202

Shaw JR, Cooper DJ (2008) Linkages among watersheds, stream reaches, and riparian vegetation in dryland ephemeral stream networks. J Hydrol 350:68–82

Sheldon F, Bunn SE, Hughes JM, Arthington AH, Balcombe SR, Fellows CS (2010) Ecological roles and threats to aquatic refugia in arid landscapes: dryland river waterholes. Mar Freshwater Res 61:885–895

Sjögersten S, Black CR, Evers S, Hoyos-Santillan J, Wright EL, Turner BL (2014) Tropical wetlands: a missing link in the global carbon cycle? Global Biogeochem Cy 28:1371–1386

Snelder TH, Datry T, Lamouroux N, Larned ST, Sauquet E, Pella H, Catalogne C (2013) Regionalization of patterns of flow intermittence from gauging station records. Hydrol Earth Syst Sc 17:2685–2699

Sonnentag O, van der Kamp G, Barr AG, Chen JM (2010) On the relationship between water table depth and water vapor and carbon dioxide fluxes in a minerotrophic fen. Glob Change Biol 16:1762–1776

Stanford JA, Ward JV (2001) Revisiting the serial discontinuity concept. Regul River 17:4–5

Steward AL, von Schiller D, Tockner K et al (2012) When the river runs dry: human and ecological values of dry riverbeds. Front Ecol Environ 10:202–209

Strahler AN (1957) Quantitative analysis of watershed geomorphology. Civ Eng 101:1258–1262

Tamooh F, Borges AV, Meysman FJ, Van Den Meersche K, Dehairs F, Merckx R, Bouillon S (2013) Dynamics of dissolved inorganic carbon and aquatic metabolism in the Tana River Basin, Kenya. Biogeosciences 10:6911–6928

Teodoru CR, Nyoni FC, Borges VA, Darchambeau F, Nyambe I, Bouillon S (2015) Dynamics of greenhouse gases (CO_2, CH_4, N_2O) along the Zambezi River and major tributaries, and their importance in the riverine carbon budget. Biogeosciences 12:2431–2453

875
876 Thauer RK, Kaster AK, Seedorf H, Buckel W, Hedderich R (2008) Methanogenic archaea:
877 ecologically relevant differences in energy conservation. Nat Rev Microbiol 6: 579–591
878
879 Threatened Species Scientific Committee (TSSC) (2005) Commonwealth Listing Advice on
880 Temperate Highland Peat Swamps on Sandstone. Australian Government Department of
881 Environment. http://www.environment.gov.au/node/14561. Accessed on 02 December 2015
882
883 Timoner X, Acuña V, von Schiller D, Sabater S (2012) Functional responses of stream biofilms
884 to flow cessation, desiccation and rewetting. Freshwater Biol 57:1565–1578.
885
886 Tweed S, Leblanc M, Bass AM, Harrington GA, Munksgaard NC, Bird MI (2016) Leaky
887 savannas: the significance of lateral carbon fluxes in the seasonal tropics. Hydrol Process 30:873–
888 887
889
890 Vachon D, Prairie YT (2013) The ecosystem size and shape dependence of gas transfer velocity
891 versus wind speed relationships in lakes. Can J Fish Aquat Sci 70:1757-1764
892
893 von Schiller D, Marcé R, Obrador B, Gómez-Gener L, Casas-Ruiz JP, Acuña V, Koschorreck M
894 (2014) Carbon dioxide emissions from dry watercourses. Inland Waters 4:377-382
895
896 von Schiller D, Graeber D, Ribot M, Timoner X, Acunã V, Martí E, Sabater S, Tockner K (2015)
897 Hydrological transitions drive dissolved organic matter quantity and composition in a temporary
898 Mediterranean stream. Biogeochemistry 123:429–446
899
900 Wanninkhof R (2014). Relationship between wind speed and gas exchange over the ocean
901 revisited. Limnol Oceanogr–Meth 12:351–362
902
903 Weiss RF (1974) Carbon dioxide in water and seawater: the solubility of a non-ideal gas. Mar
904 Chem 2(3):203–215
905
906 Weyhenmeyer GA, Kortelainen P, Sobek S, Müller R, Rantakari M (2012) Carbon dioxide in
907 boreal surface waters: a comparison of lakes and streams. Ecosystems 15:1295–1307
908
909 Weyhenmeyer GA, Kosten S, Wallin MB, Tranvik LJ, Jeppesen E, Roland F (2015) Significant
910 fraction of CO_2 emissions from boreal lakes derived from hydrologic inorganic
911 carbon inputs. Nat Geosci 8:933-936
912
913 Xia J, Wu B, Wang G, Wang Y (2010) Estimation of bankfull discharge in the Lower Yellow
914 River using different approaches. Geomorphology 117:66–77
915
916 Yamamoto S, Alcauskas JB, Crozier TE (1976) Solubility of methane in distilled water and
917 seawater. J Chem Eng Data 21:78–80
918
919 Yvon-Durocher G, Allen AP, Bastviken D et al (2014) Methane fluxes show consistent
920 temperature dependence across microbial to ecosystem scales. Nature 507:488–491
921
922
923
924
925

Fig. 1 Map of the upper Jamison Creek watercourse and study sites S1-S5. Source: ArcGIS 10.3. (ESRI; Redlands, CA)

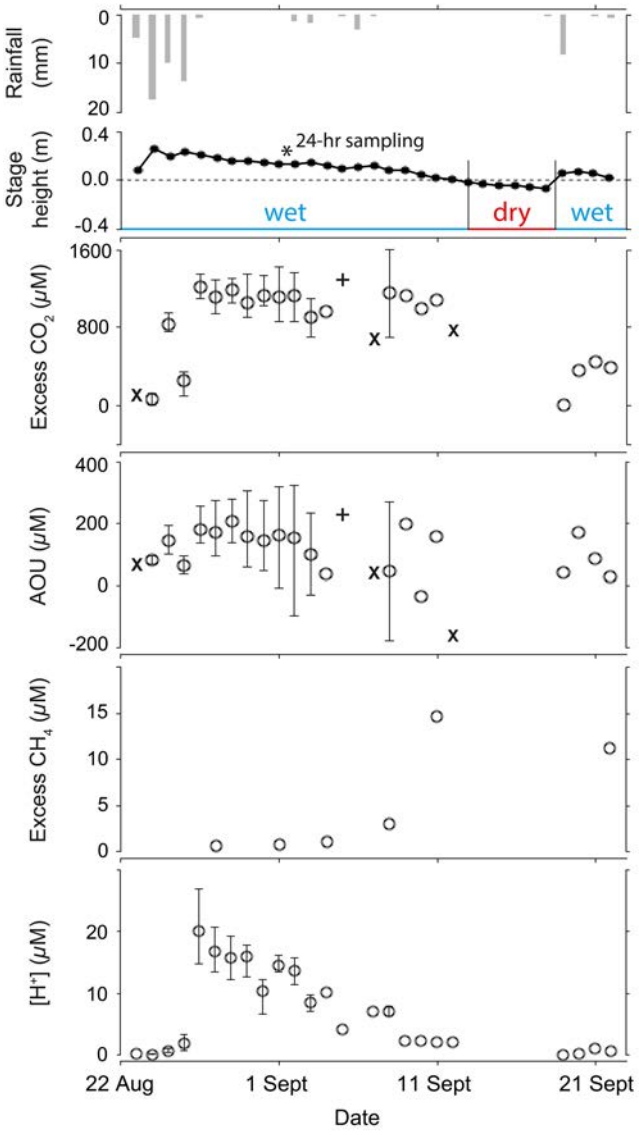

Fig. 2 Time series measurements of excess CO_2, AOU, excess CH_4 and [H^+] taken over the initial two wet-cycles at the S1 study segment. Where $n \geq 2$, error bars indicate the range for each variable. Where $n = 1$, + indicates samples collected between 06:00-10:00 hrs, O indicates samples collected between 10:00-12:30 hrs, and X indicates samples collected between 12:30-19:00 hrs

936

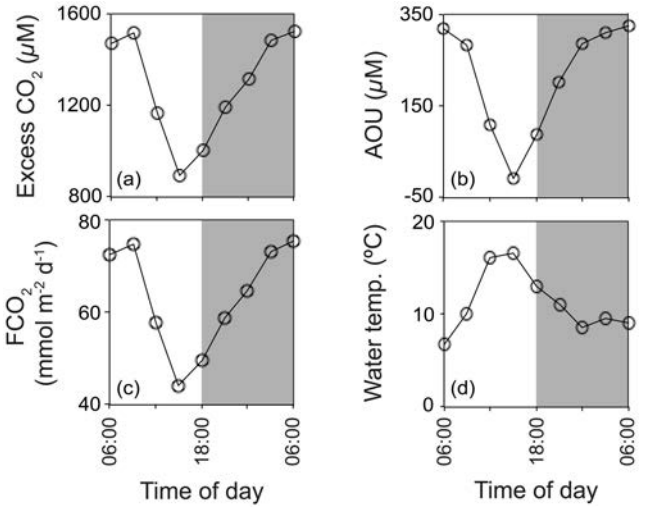

937
938 **Fig. 3** Diel measurements of (a) excess CO_2, (b) the apparent oxygen utilisation (AOU), (c) the CO_2-C flux
939 rate, and (d) water temperature at the S1 study segment during a period of low stage height, 10 days post-
940 rewetting
941
942
943
944
945

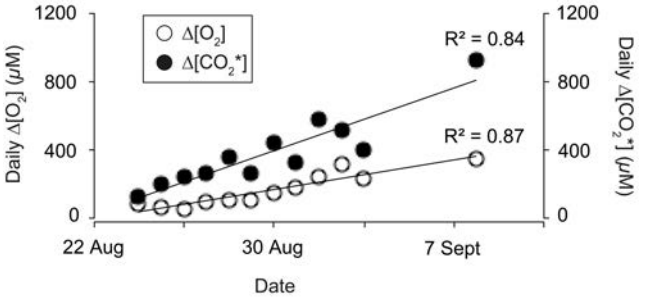

946
947
948 **Fig. 4** Time series of daily change in concentration (Δ) for $[O_2]$ and $[CO_2^*]$ taken at the S1 timeseries
949 station during the initial, longer wet-to-dry cycle

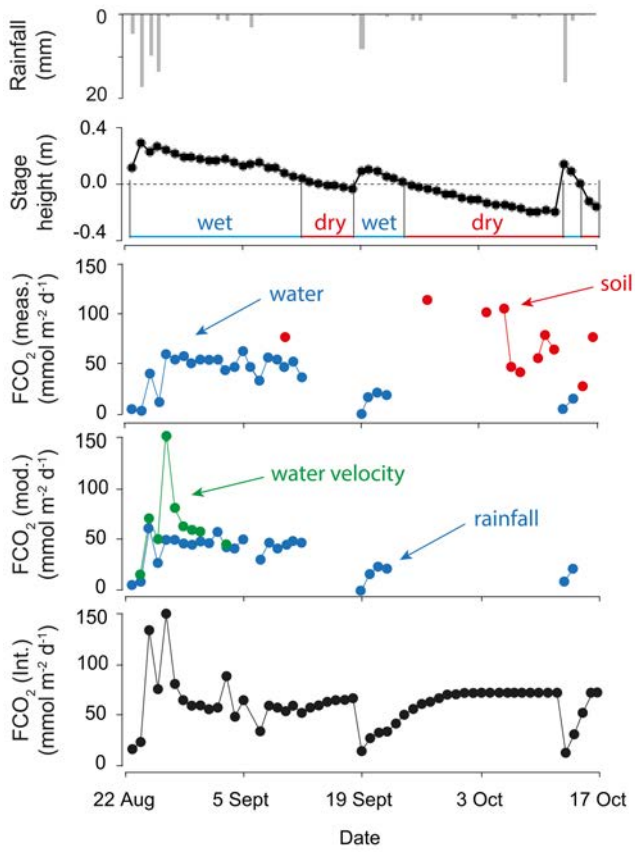

Fig. 5 Time series measurements of mean daily rainfall and stage height, measured and modelled CO_2-C fluxes, as well as integrated water- and soil-air fluxes

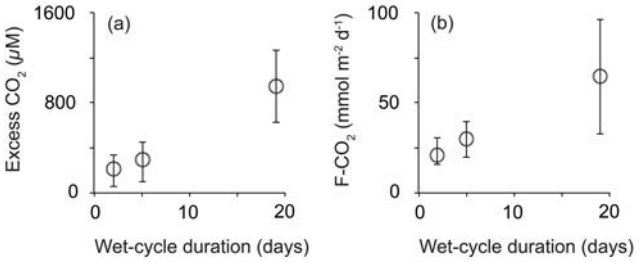

Fig. 6 The relationship between wet-cycle duration and (a) mean daily water column excess CO_2 concentrations, as well as (b) integrated water and soil-air CO_2-C fluxes. Error bars indicate the standard deviations for each cycle

964

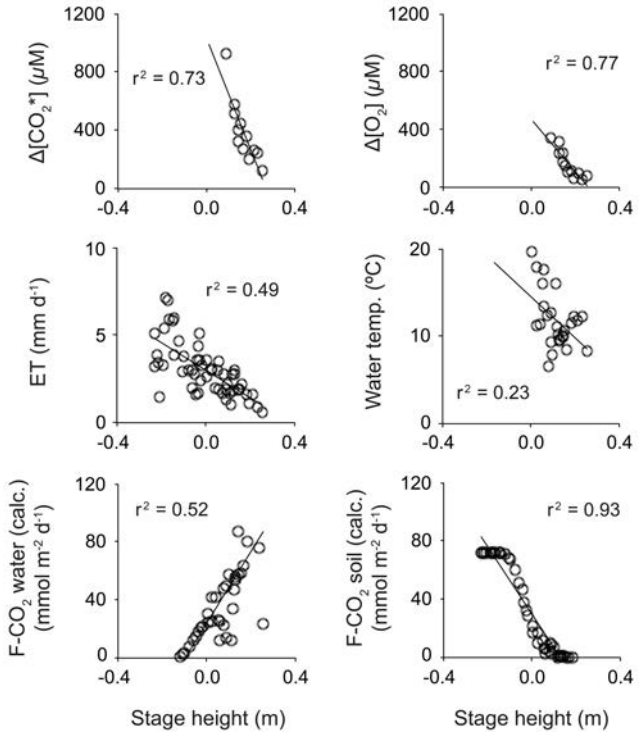

965
966
967
968
969
970
971

Fig. 7 Relationships between mean stage height with $\Delta[CO_2^*]$, $\Delta[O_2]$, evapotranspiration rate (ET), water temperature, as well as the calculated total water and soil ratio-corrected CO_2-C fluxes per daily time step at the S1 study site

972
973
974
975

Table 1 Mean between-site variability in water quality parameters (±SD), apparent oxygen utilisation (AOU), excess CO_2, excess CH_4, mean water-air flux rates (F) for CO_2 and CH_4, and water column morphology for study sites S1-S5 during the two days of spatial sampling

Site	Water temp. (°C)	pH	Sp. Cond. (μs cm^{-1})	AOU (μM)	Excess CO_2 (μM)	Excess CH_4 (μM)	F-CO_2 (mmol C m^{-2} d^{-1})	F-CH_4 (mmol C m^{-2} d^{-1})	Wetted length (m)	Wetted width (m)	Stage height (m)
S1	14.5 ±4.7	5.87 ±0.31	89 ±6	93 ±91	733 ±495	12.9 ±2.4	36.0 ±24.3	1.7 ±0.3	14.4	1.0	0.1
S2	10.2 ±0.6	6.05 ±0.43	101 ±6	265 ±56	531 ±389	2.6 ±0.9	26.1 ±19.1	0.3 ±0.1	2.4	2.1	0.2
S3	13.2 ±1.0	5.52 ±0.48	72 ±3	155 ±0	1390 ±227	0.4 ±0.0	68.3 ±11.2	0.1 ±0.0	16.2	0.5	0.3
S4	14.9 ±0.4	5.63 ±0.32	70 ±3	114 ±1	760 ±61	6.4 ±2.8	37.4 ±3.0	0.9 ±0.4	8.4	1.6	0.4
S5	15.0 ±0.5	5.89 ±0.40	61 ±2	120 ±23	326 ±32	4.3 ±0.7	16.0 ±1.6	0.6 ±0.1	5.7	1.2	0.4

976
977
978
979
980
981
982

983
984
985
986

Table 2 Comparison summary of mean CO_2 concentration and fluxes for temporary ponds, perennial flowing rivers and streams, seasonally ephemeral watercourses, lakes, and wetlands worldwide (±SD; ranges shown in parentheses)

Location/ watercourse type	**Flux Wet[f] (mmol m^{-2} d^{-1})**	**Flux Wet[s] (mmol m^{-2} d^{-1})**	**Flux Dry (mmol m^{-2} d^{-1})**	**Reference**
River Fluvià, Spain/ seasonally ephemeral	22[*] (11–26)	7[*] (6–11)	58[*] (10–124)	von Schiller et al. 2014
Iberia, Spain/ seasonally ephemeral	83±56	-	213±106 (93–418)	Gómez-Gener et al. 2016
Tucson, Arizona/ seasonally ephemeral	-	-	44±8[p,se,v] (20-3173)	Gallo et al. 2013
Worldwide / small ponds < <0.001 km^2	-	35±5[m,se]	-	Holgerson 2016
Mediterranean/ temporary ponds	-	3 (1-11)	(2-96)[v]	Catalán et al. 2014
Worldwide/ flowing waters	766[m]	-	-	Raymond et al. 2013
Conterminous USA / flowing waters	541±182[m] (201-914)	-	-	Butman & Raymond 2011
Boreal/ lakes	-	33[m]	-	Weyhenmeyer et al. 2015
Worldwide/ lakes and reservoirs	-	7[m] (1-17)	-	Raymond et al. 2013
Tropical/ wetlands[¶]	-	107±50[p,v] (20-141)	255±111[p,v] (69-493)	Sjögersten et al. 2014 (table 4)
Boreal/ fen[¶¶]	-	117[p,v]	144[p,v]	Sonnentag et al. 2010
This study	67±38[m] (-9 to 349)	30±20 (0-62)	72±27[v] (27-115)	

987
988
989